Technical Notes

Multi-Objective Optimization of a Transonic Compressor Rotor by Using an Adjoint Method

Jiaqi Luo*
Peking University, 100871 Beijing, People's Republic of China
and
Feng Liu†
University of California, Irvine, California 92697-3975

DOI: 10.2514/1.J053436

I. Introduction

TO IMPROVE the aerodynamic performance and the economic benefits of an aircraft engine, one strives to increase the total pressure ratio, the adiabatic efficiency et al., and decrease the size and weight of the engine. Multi-objective optimization has been proposed and studied to satisfy the higher-level requirements in recent years. Benini [1] successfully performed the multi-objective optimization of the NASA Rotor 37 to maximize the total pressure ratio and the compressor efficiency by using a multi-objective evolutionary algorithm. Lian and Liou [2] redesigned the blade of NASA Rotor 67 to maximize the total pressure ratio while minimizing the compressor weight, and an approximately 1.8% total pressure ratio gain was achieved.

Because of its robustness and excellent compatibility in design optimization, the nongradient-based optimization methods, such as evolutionary algorithm and the surrogate model-based methods [1–4] have been widely applied to the design optimization. The nongradient-based design optimization can support the global optimum in a wide design space. However, for the design optimization of complex aerodynamic shapes, numerous flow calculations are necessary because of the large number of design parameters. The adjoint method proposed by Jameson [5] can support the gradient information fast for the gradient-based design optimization. The design optimization by using the adjoint method can significantly improve the computational efficiency because it requires about only two flow calculations in each design cycle to determine the complete gradient information of each cost function, regardless of the number of design parameters. In the past decades, the adjoint method was widely used in the design optimization of external flow. Jameson and Reuther [6,7] successfully performed aerodynamic design optimization of airfoil, wing, and wing–body configuration by using a continuous adjoint method. In recent years, this method has been introduced to the design optimization of turbomachinery blades by Dreyer and Martinelli [8] and Yang et al. [9]. Recently, by using the adjoint method, the aerodynamic shape design optimization [10], the multistage design optimization [11,12], the aeroelastic design optimization [13], and the multipoint design optimization [14] of turbomachinery blades are successfully performed.

Because of its high efficiency and sufficient accuracy on gradient calculation, the adjoint method has already been used in the multi-objective design optimization [15–17]. A simple but widely used approach for the gradient-based multi-objective optimization is the weighted-sum method with a single cost function consisting of a linear combination of multiple cost functions with appropriate weights, which converts the multi-objective optimization problem into a single-objective optimization problem. However, as pointed out by Shankaran and Barr [15], this method is unable to capture the concave portions and the disjoint Pareto fronts. Furthermore, this method cannot always guarantee sufficient design convergence because the improvement of some objectives brings with it unexpected defects not allowed in reality. For example, in the multi-objective optimization of total pressure ratio and adiabatic efficiency of a transonic compressor rotor, the total pressure ratio is not allowed to increase without limit because increasing total pressure ratio induces 1) increased turning to a critical degree, after which the mass flow rate decreases away from the constraint, and 2) compressor stall triggers at a lower backpressure due to the stronger shock and the more intensive shock/tip-leakage interaction. The detrimental performance brings difficulties on obtaining the optimal aerodynamic shape.

To overcome the drawbacks of the traditional gradient-based multi-objective optimization mentioned previously, an approach for multi-objective optimization is introduced in the present study. The multi-objective optimization is decomposed into two steps. The first step favors obtaining a series of initialized blades avoiding the compressor stall triggers at the design condition, and the second step, consisting of a series of single-objective optimizations, favors determining the Pareto front. The aerodynamic shape of a transonic compressor rotor NASA Rotor 67 is redesigned at the operating condition near peak efficiency to maximize the total pressure ratio and the adiabatic efficiency with the constraint of mass flow rate by using the adjoint method. The Pareto front of the multi-objective optimization is finally given, and the effects of blade profile modification on the performance improvement are presented.

II. Adjoint Method

The adjoint method can be introduced conceptually as following. Let $I(\boldsymbol{w}, \mathcal{F})$ be the cost function depending on the flowfield $\boldsymbol{w}$ and the geometry $\mathcal{F}$; and the variation of the cost function δI consists of two parts, one due to the variation of flowfield $\delta\boldsymbol{w}$ and the other due to the variation of geometry $\delta\mathcal{F}$. In the meantime, $\delta\boldsymbol{w}$ is implicitly dependent on $\delta\mathcal{F}$ through the governing flow equation $\boldsymbol{R}(\boldsymbol{w}, \mathcal{F}) = 0$, which is the Reynolds-averaged Navier–Stokes (RANS) equation in the present study. By introducing a series of adjoint variables Ψ and then subtracting the product of Ψ^T with $\delta\boldsymbol{R}(\boldsymbol{w}, \mathcal{F})$ from the variation of the cost function, we get

$$\delta I = \left\{\frac{\partial I}{\partial \boldsymbol{w}} - \Psi^T \frac{\partial \boldsymbol{R}}{\partial \boldsymbol{w}}\right\}\delta\boldsymbol{w} + \left\{\frac{\partial I}{\partial \mathcal{F}} - \Psi^T \frac{\partial \boldsymbol{R}}{\partial \mathcal{F}}\right\}\delta\mathcal{F} \tag{1}$$

The key of the adjoint method is to eliminate the contribution of $\delta\boldsymbol{w}$ to δI to avoid calculating $\delta\boldsymbol{w}$ for each $\delta\mathcal{F}$. This can be achieved if Ψ satisfies the adjoint equation

Presented as Paper 2013-2732 at the 43rd AIAA Fluid Dynamics Conference and Exhibit, San Diego, CA, 24–27 June 2013; received 28 February 2014; revision received 25 June 2014; accepted for publication 25 June 2014; published online 19 September 2014.

*Research Associate, Department of Aeronautics and Astronautics; jiaqil@pku.edu.cn.

†Professor, Department of Mechanical and Aerospace Engineering; fliu@uci.edu. Fellow AIAA.

$$\frac{\partial I}{\partial \boldsymbol{w}} - \Psi^T \frac{\partial \boldsymbol{R}}{\partial \boldsymbol{w}} = 0 \tag{2}$$

Then, we have $\delta I = \boldsymbol{G}\delta\mathcal{F}$, where

$$\boldsymbol{G} = \frac{\partial I}{\partial \mathcal{F}} - \Psi^T \frac{\partial \boldsymbol{R}}{\partial \mathcal{F}} \tag{3}$$

is the gradient of I with respect to $\delta\mathcal{F}$. Once the flow variables $\boldsymbol{w}$ and the adjoint variables Ψ are obtained through solving the flow-governing equation and the corresponding adjoint equation each once, the gradient can then be calculated after obtaining some additional grid deformation information using a direct finite-difference method, which costs little computer time.

The derivations and the formulation of the adjoint equations corresponding to the RANS equations, the numerical method for solving the continuous adjoint equations, and the adjoint gradient calculation have already been demonstrated [18]. The accuracy of the gradients is the most important for the design optimization by using the gradient-based methods. Although the gradients of the discrete adjoint method are more accurate, the gradients of the continuous adjoint method have already been computed and compared with those obtained from the finite-difference method, demonstrating an acceptable accuracy [9,14,18].

III. Descriptions of Multi-Objective Optimization

A. Rotor 67 Flow Validation

NASA Rotor 67 is a transonic axial-flow compressor blade in the first-stage rotor of a two-stage fan, which was developed in the 1970s and was then experimentally investigated. In the present paper, the RANS equations with a source term and the Spalart–Allmaras one-equation turbulence model equation are solved to simulate the turbomachinery flow. A simple periodicity clearance model is used. An H-grid containing 120, 48, and 44 cells in the axial, pitchwise, and spanwise directions, respectively, is used for flow calculations. The computational results have already been compared with the experimental results [19], and an excellent agreement was achieved [14].

B. Multi-Objective Optimization

The multi-objective optimization studied in the present paper is completed by two steps in the following, which are referenced as design initialization and Pareto front determination, respectively.

The design initialization attempts to maximize the total pressure ratio with the constraint of mass flow rate. The cost function is defined as

$$I = \frac{1}{\pi} + \Lambda|\sigma - 1| \tag{4}$$

with the subject

$$1 \le \hat{\pi} = \frac{\pi}{\pi_0} \le \hat{\pi}_{\max} \tag{5}$$

where σ denotes the ratio of mass flow rate; Λ is the coefficient of the penalty function; π and π_0 are the total pressure ratio of the redesigned and the reference blades, respectively; $\hat{\pi}$ is the ratio of total pressure ratio; and $\hat{\pi}_{\max}$ is the upper limit. The design initialization is one kind of quasi-single-objective design optimization to maximize the total pressure ratio starting from the original blade of Rotor 67. As the design optimization progresses, a set of redesigned blades with different gains of total pressure ratio are selected instead of obtaining the optimal blade profile of a real single-objective optimization. These redesigned blades are named as initialized blades. Through the operation performance analysis of all the initialized blades, the upper limit $\hat{\pi}_{\max}$ can be approximately determined to avoid the compressor stall triggers at the design condition.

The Pareto front determination involves a set of single-objective optimizations, each of which starts from the corresponding initialized blade to maximize the adiabatic efficiency. High-efficiency means low flow loss, and all kinds of flow losses can be measured by entropy production. The entropy production per unit mass flow rate is selected as the cost function herein. Constraints on mass flow rate and total pressure ratio are enforced by incorporating penalty functions in the cost function. The cost function with constraints is given as

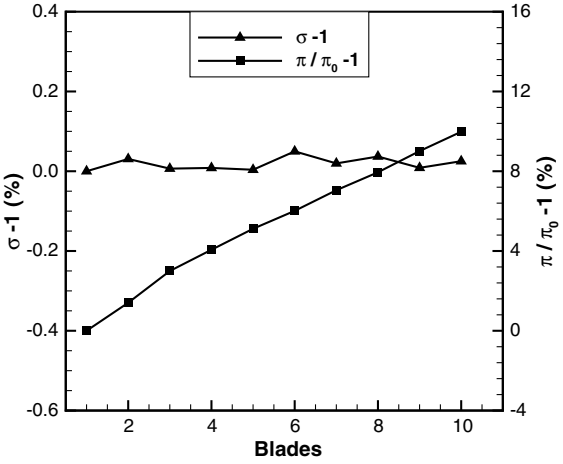

Fig. 1 Variations of mass flow rate and total pressure ratio.

$$I = s_{\text{gen}} + \Lambda_1|\sigma - 1| + \Lambda_2|\hat{\pi} - 1| \tag{6}$$

where s_{gen} denotes the entropy production per unit mass flow rate. Minimization of the cost function described previously attempts to obtain an optimized blade profile that maximizes the adiabatic efficiency for the same total pressure ratio and mass flow rate.

The fundamental principle of the introduced approach is to decompose the multi-objective optimization into a multistep single-objective optimization. The step number of the single-objective optimization is strictly dependent on the number of the design objectives. Suppose that there are more objectives in the design optimization; the single-objective optimization can be performed step-by-step with increasing number of constraints.

In both the design initialization and the Pareto front determination, the profiles of nine blade sections along the span are selected to be redesigned. Hicks–Henne shape functions [20] are introduced to perturb the reference blade profile, and 16 shape functions are uniformly distributed each on the pressure and the suction surfaces at each of the selected blade sections.

On obtaining the adjoint gradients, a simple steepest-descent optimization method is used to not only exempt from additional flow calculations but also ensure the design convergence, which cannot be achieved by using most of the other gradient-based optimization methods. With a given step length, the variations of the design parameters can be determined in the opposite direction of the adjoint gradients, and then the blade profile can be renewed for the next design cycle.

IV. Results and Discussion

A. Design Initialization

Design initialization is performed to obtain a set of initialized blades without stall triggers at the design condition. The coefficient of the penalty function as shown in Eq. (4) is $\Lambda = 0.4$.

Figure 1 presents the variations of mass flow rate and total pressure ratio of the initialized blades obtained by a selection process in the design initialization. These blades are named from Blade_1 to Blade_10 in turn; and Blade_1 is the original blade of Rotor 67. The mass flow rate is strictly enforced for all the initialized blades, with the maximum discrepancy not exceeding 0.05%. Compared with Blade_1, the increment of total pressure ratio increases from about 1.4% of Blade_2 to about 10% of Blade_10.

Figure 2 presents the overall performance of Blade_1, Blade_3, Blade_6, and Blade_7. Design initialization through blade profile modification contributes significant increment of total pressure ratio

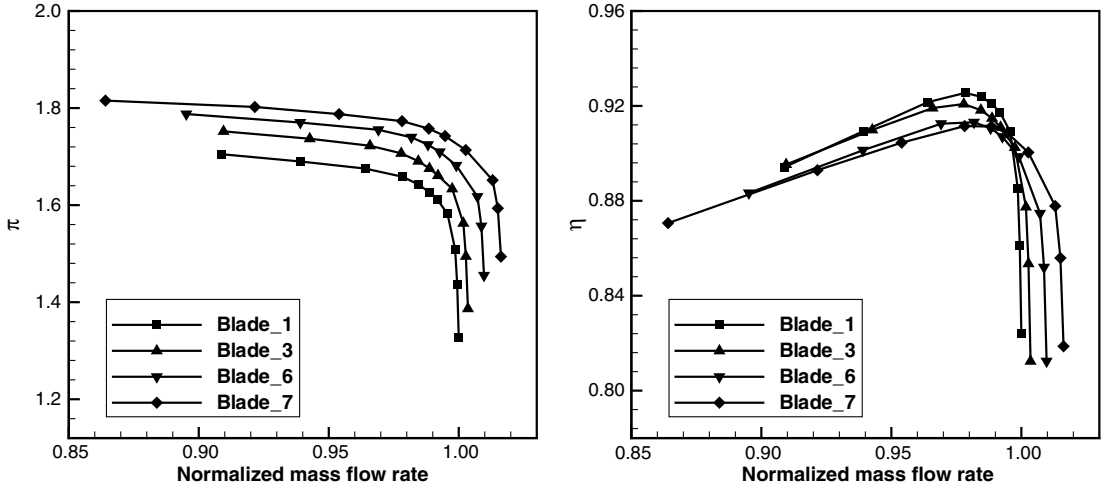

a) Total pressure ratio **b) Adiabatic efficiency**

Fig. 2 Operating characteristics of the initialized blades.

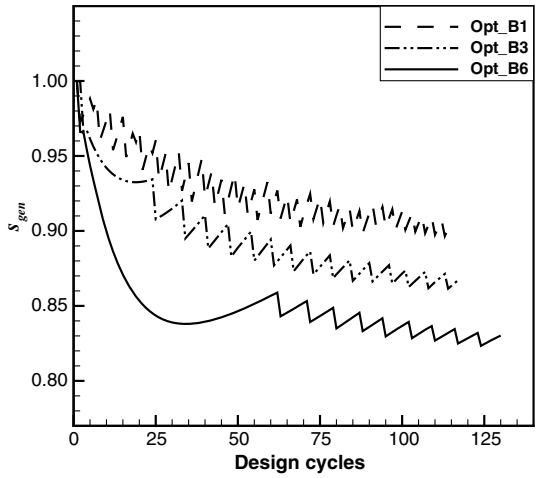

Fig. 3 Cost function vs design cycles.

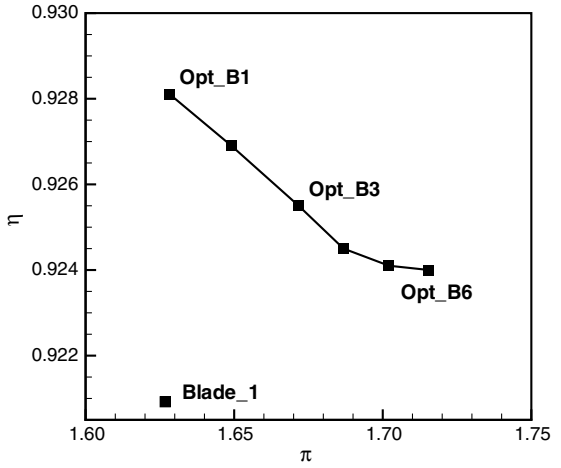

Fig. 4 Pareto front.

and significant decrement of adiabatic efficiency to the initialized blades over the full operating range, compared with those of Blade_1. Although the present steady-state CFD approaches cannot accurately capture the true stall, the magnitude of the decrement of either mass flow rate or adiabatic efficiency near stall is usually regarded as one of the means to predict stall. Besides, the steady flow computation near stall usually converges slowly. In this figure, the mass flow rate of Blade_7 performs a larger decline rate than other initialized blades with the same backpressure increment and even performs a noticeable decrease at the operating condition near peak efficiency. Consequently, an upper limit of about 7% for the total pressure ratio increment is given herein. The initialized blades from Blade_1 to Blade_6 are selected to be optimized to determine the Pareto front.

B. Pareto Front Determination

The single-objective optimizations starting from the initialized blades seek to find the optimums to construct the Pareto front of the multi-objective optimization. Nemec et al. [16] performed the multi-objective optimization of an airfoil by using the adjoint method, and the Pareto solutions were obtained following the proposed convergence criterion that the L_2 norm of the adjoint gradient should be less than 0.01. The present single-objective optimization is performed with another convergence criterion:

$$\left| \frac{s_{\text{gen},i+1}}{s_{\text{gen},i}} - 1 \right| \leq \delta_s \tag{7}$$

where $s_{\text{gen},i}$ and $s_{\text{gen},i+1}$ are the entropy production of the adjacent optimized profiles satisfying

$$|\sigma - 1| \leq \delta_m, \qquad |\hat{\pi} - 1| \leq \delta_\pi \tag{8}$$

and $\delta_s = 0.5\%$, $\delta_m = 0.05\%$, and $\delta_\pi = 0.5\%$ in the present study.

Figure 3 presents the entropy production per unit mass flow rate versus design cycles for three optimized blades, where the entropy production is normalized by the corresponding reference value. Opt_B1, Opt_B3, and Opt_B6 denote the optimized blades of the single-objective optimizations starting from Blade_1, Blade_3, and Blade_6, respectively. Within less than 130 design cycles, the entropy production approaches convergence.

Figure 4 presents the Pareto front of the multi-objective optimization. The adiabatic efficiency significantly increases without loss in total pressure ratio for all the optimized blades due to the lower

Table 1 Performance of both initialized and optimized blades

Blade	s_{gen}	$\dot{m}$, kg/s	π	η, %	β, deg
Blade_1	1.000	34.59	1.627	92.09	−38.85
Blade_3	1.140	34.59	1.675	91.48	−41.09
Blade_6	1.261	34.57	1.724	91.06	−43.19
Opt_B1	0.906	34.59	1.628	92.81	−38.81
Opt_B3	0.967	34.60	1.672	92.55	−40.75
Opt_B6	0.988	34.59	1.716	92.46	−42.58

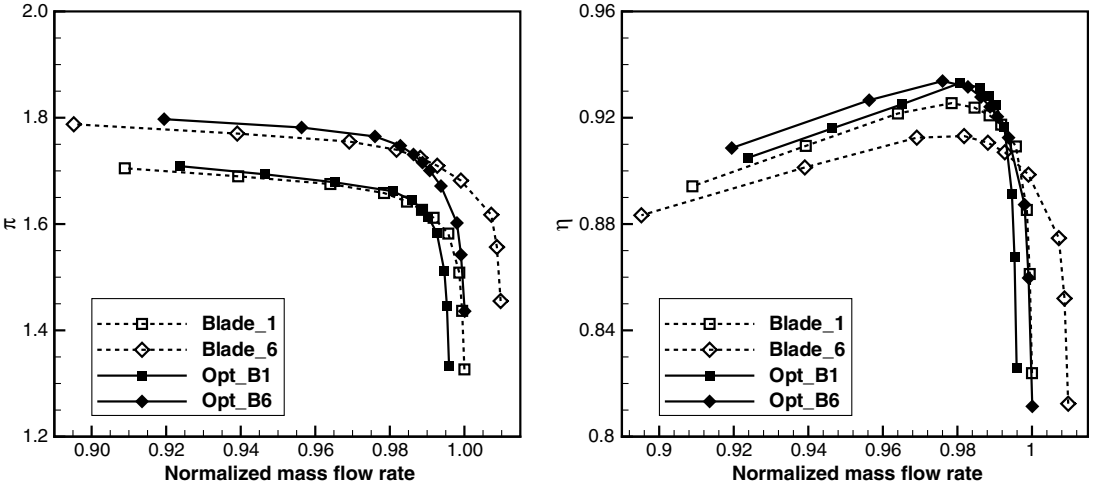

a) Total pressure ratio **b) Adiabatic efficiency**

Fig. 5 Operating characteristics of both initialized and optimized blades.

limit of total pressure ratio as presented in Eq. (5). As total pressure ratio increases, the adiabatic efficiency decreases. Supposing the total pressure ratio is allowed to be lower than that of the original blade of Rotor 67, more gains of adiabatic efficiency can be achieved.

To investigate the influence of blade profile modification on the performance improvement, the flow solutions of six different blades are presented and compared in detail. Table 1 gives the flow solutions of both the initialized and the optimized blades. The entropy production is normalized by that of Blade_1, and the mass flow rate of all the blades maintains almost the same. As the total pressure ratio increases through design initialization, the shock wave appears to be stronger, resulting in more flow loss along with increased entropy production and decreased adiabatic efficiency. In the meantime, the flow turning increases due to the improved working capability. Through blade optimization, the adiabatic efficiency of each optimized blade is increased with strictly enforced mass flow rate and total pressure ratio. Compared with that of the corresponding initialized blade, the flow turning of each optimized blade is decreased.

Figure 5 presents the overall performance of the initialized and the optimized blades. Compared with each of the corresponding initialized blades, the total pressure ratio of each of the optimized blades increases below 98% normalized mass flow rate, whereas it performs a slight change around the 98% normalized mass flow rate and beyond. However, the adiabatic efficiency increases over almost the whole operating range. Compared with the original blade of Rotor 67, both the total pressure ratio and the adiabatic efficiency of Opt_B6 significantly increase over almost the whole operating range through the present multi-objective optimization design.

Experiment [19] suggests that Rotor 67 approaches stall at about 93% normalized mass flow rate. The true stall cannot be captured in the present study. Reasons include the following.

1) The steady-state flow model might not be able to simulate the high unsteady stall flow and consequently cannot capture the real stall phenomena.

2) The numerical simulation of leakage flow is still an open issue, and different turbulence models may support quite different results, as shown by Biollo and Benini [21].

Whether the multi-objective optimization offers a wider stall margin cannot be confirmed by the present steady-state code. However, as presented in Fig. 5, the decrement of mass flow rate of Opt_B1 and Opt_B6 below 98% normalized mass flow rate is much less than that of Blade_1 and Blade_6, respectively, which indicates that potential extension of stall margin can be obtained.

V. Conclusions

An approach for the gradient-based multi-objective optimization is introduced, and the blade profile of NASA Rotor 67 is redesigned to maximize the total pressure ratio and the adiabatic efficiency by using a continuous adjoint method. The multi-objective optimization is completed by two steps: design initialization and Pareto front determination. The design initialization maximizing total pressure ratio alone supports a set of initialized blades and an approximate upper limit of total pressure ratio, which is verified to be necessary in the present multi-objective optimization to avoid stall triggers at the design condition. A series of single-objective optimizations starting from the initialized blades are successfully performed to maximize the adiabatic efficiency with the constraints of mass flow rate and the corresponding initialized total pressure ratio. A limited number of Pareto solutions are obtained at the design convergence of the single-objective optimization, and thus the Pareto front is determined. The results demonstrate that, through the proposed multi-objective optimization, both the total pressure ratio and the adiabatic efficiency increase over almost the whole operating range compared with those of the original blade, and the stall margin can be potentially extended.

Acknowledgments

The authors would like to thank the National Natural Science Foundation of China (grant numbers 51206003 and 51376009) and the National Science Foundation for Postdoctoral Scientists of China (grant numbers 2012M510267 and 2013T60035) for supporting this research work.

References

[1] Benini, E., "Three-Dimensional Multi-Objective Design Optimization of a Transonic Compressor Rotor," *Journal of Propulsion and Power*, Vol. 20, No. 3, 2004, pp. 559–565. doi:10.2514/1.2703

[2] Lian, Y., and Liou, M. S., "Multi-Objective Optimization of Transonic Compressor Blade Using Evolutionary Algorithm," *Journal of Propulsion and Power*, Vol. 21, No. 6, 2005, pp. 979–987. doi:10.2514/1.14667

[3] Simpson, T. W., Mauery, T. M., Korte, J. J., and Mistree, F., "Kriging Models for Global Approximation in Simulation-Based Multidisciplinary Design Optimization," *AIAA Journal*, Vol. 39, No. 12, 2001, pp. 2233–2241. doi:10.2514/2.1234

[4] Duan, Y., Cai, J., and Li, Y., "Gappy Proper Orthogonal Decomposition-Based Two-Step Optimization for Airfoil Design," *AIAA Journal*, Vol. 50, No. 4, 2012, pp. 968–971. doi:10.2514/1.J050997

[5] Jameson, A., "Aerodynamic Design via Control Theory," *Journal of Scientific Computing*, Vol. 3, No. 3, 1988, pp. 233–260. doi:10.1007/BF01061285

[6] Jameson, A., and Reuther, J., "Control Theory Based Airfoil Design Using the Euler Equations," *5th Symposium on Multidisciplinary Analysis and Optimization*, AIAA Paper 1994-4272, 1994.

[7] Reuther, J., and Jameson, A., "Aerodynamic Shape Optimization of Wing and Wing-Body Configurations Using Control Theory," *33rd Aerospace Sciences Meeting and Exhibit*, AIAA Paper 1995-0123, Jan. 1995.

[8] Dreyer, J. J., and Martinelli, L., "Hydrodynamic Shape Optimization of Propulsor Configurations Using a Continuous Adjoint Approach," *15th AIAA Computational Fluid Dynamics Conf.*, AIAA Paper 2001-2580, June 2001.

[9] Yang, S., Wu, H., Liu, F., and Tsai, H. M., "Aerodynamic Design of Cascades by Using an Adjoint Equation Method," *41st Aerospace Sciences Meeting and Exhibit*, AIAA Paper 2003-1068, Jan. 2003.

[10] Luo, J., Xiong, J., Liu, F., and McBean, I., "Three-Dimensional Aerodynamic Design Optimization of a Turbine Blade by Using an Adjoint Method," *ASME Journal of Turbomachinery*, Vol. 133, No. 1, 2011, Paper 011026. doi:10.1115/1.4001166

[11] Wang, D., and He, L., "Adjoint Aerodynamic Design Optimization for Blades in Multi-Stage Turbomachines: Part 2—Validation and Application," *ASME Journal of Turbomachinery*, Vol. 132, No. 2, 2010, Paper 021012. doi:10.1115/1.3103928

[12] Walther, B., and Nadarajah, S., "Constrained Adjoint-Based Aerodynamic Shape Optimization of a Single-Stage Transonic Compressor," *ASME Journal of Turbomachinery*, Vol. 135, No. 3, 2013, Paper 021017. doi:10.1115/1.4007502

[13] He, L., and Wang, D., "Concurrent Blade Aerodynamic-Aeroelastic Design Optimization Using Adjoint Method," *ASME Journal of Turbomachinery*, Vol. 133, No. 1, 2011, Paper 011021. doi:10.1115/1.4000544

[14] Luo, J., Zhou, C., and Liu, F., "Multi-Point Design Optimization of a Transonic Compressor Blade by Using an Adjoint Method," *ASME Journal of Turbomachinery*, Vol. 136, No. 5, 2014, Paper 051005. doi:10.1115/1.4025164

[15] Shankaran, S., and Barr, B., "Efficient Gradient-Based Algorithm for the Construction of Pareto Front," *ASME Turbo Expo 2011: Turbine Technical Conference and Exposition*, American Soc. of Mechanical Engineers Paper GT2011-45069, Fairfield, NJ, 2011.

[16] Nemec, M., Zingg, D. W., and Pulliam, T. H., "Multipoint and Multi-Objective Aerodynamic Shape Optimization," *AIAA Journal*, Vol. 42, No. 6, 2004, pp. 1057–1065. doi:10.2514/1.10415

[17] Kee Lee, C. J., Furuya, W., Tanaka, M., and Takano, N., "Adjoint Variable Method for Multi-Objective Sizing and Shape Optimization," *Journal of Computational Science and Technology*, Vol. 3, No. 1, 2009, pp. 275–286. doi: 10.1299/jcst.3.275

[18] Luo, J., Xiong, J., and Liu, F., "Aerodynamic Design Optimization by Using a Continuous Adjoint Method," *Science China: Physics, Mechanics and Astronomy*, Vol. 57, No. 7, 2014, pp. 1363–1375. doi:10.1007/s11433-014-5479-0

[19] Strazisar, A. J., Wood, J. R., Hathaway, M. D., and Suder, K. L., "Laser Anemometer Measurements in a Transonic Axial-Flow Fan Rotor," NASA TP-2879, 1989.

[20] Hicks, R. M., and Henne, P. A., "Wing Design by Numerical Optimization," *Journal of Aircraft*, Vol. 15, No. 7, 1978, pp. 407–412. doi:10.2514/3.58379

[21] Biollo, R., and Benini, E., "Shock/Boundary-Layer/Tip-Clearance Interaction in a Transonic Rotor Blade," *Journal of Propulsion and Power*, Vol. 25, No. 3, 2009, pp. 668–677. doi:10.2514/1.39541

J. Martins
Associate Editor